# A Multimaterial Topology Optimization considering the PM Nonlinearity

Théodore Cherrière, Tom Vancorsellis, Sami Hlioui, Luc Laurent, François Louf, H. Ben Ahmed, Mohamed Gabsi

# A Multimaterial Topology Optimization considering the PM Nonlinearity

Théodore Cherrière*,[a]
Tom Vancorsellis[a]
Sami Hlioui[b]
Luc Laurent[c,d]
François Louf[e]
Hamid Ben Ahmed[f]
Mohamed Gabsi[a]

[a] SATIE laboratory, ENS Paris-Saclay, CNRS, Université Paris-Saclay, 91190 Gif-sur-Yvette, France
[b] SATIE Laboratory, CY Cergy Paris University, CNRS, Paris-Saclay University, 95000 Cergy, France
[c] Laboratoire de Mécanique des Structures et des Systèmes Couplés, EA 3196, Conservatoire national des arts et métiers, F-75003 Paris, France
[d] HESAM University, Paris, France
[e] LMPS - Laboratoire de Mécanique Paris-Saclay, Université Paris-Saclay, CentraleSupélec, ENS Paris-Saclay, CNRS, 91190 Gif-sur-Yvette, France
[f] SATIE Laboratory, ENS Rennes, CNRS, 35170 Bruz, France
* Corresponding author
theodore.cherriere@ens-paris-saclay.fr

**Abstract**

Density-based topology optimization methodologies in magnetostatics interpolate either the magnetic permeability $\mu$ or the magnetic reluctivity $\nu$ to define intermediate materials and compute the problem sensitivities. These choices may lack physical interpretation and are not suited to model realistic permanent magnets. This work proposes the interpolation of the vector magnetic polarization $\boldsymbol{m}$ as a more general alternative, which can model any magnetic material. It is then applied to the multi-material topology optimization of the rotor of a permanent magnet synchronous machine. The case of an ideal permanent magnet with a constant magnetic polarization is compared to that of AlNiCo. The results show that considering the non-linearity of the permanent magnet can significantly impact the optimized geometry.

**Keywords:** Density Method –Multi-Material Topology Optimization – Magnetic Polarization – Nonlinear Magnetostatics – Permanent Magnet Synchronous Machine


- Doi: 10.1109/TMAG.2023.3256003

# Contents

**1. Introduction** **2**

**2. Physical analysis of the interpolations** **3**
2.1. Serial assembly - $\nu$ interpolation . . . 4
2.2. Parallel assembly - $\mu$ interpolation . . . 5
2.3. $m$-interpolation . . . 5
2.4. Discussion . . . 6

**3. Numerical implementation** **7**
3.1. Magnetic materials behavior . . . 7
3.2. 2D magnetostatics with **m**-formulation . . . 8

**4. Optimization formalism** **8**
4.1. Multi-material interpolation . . . 8
4.2. Objective function . . . 9
4.3. Optimization problem . . . 9

**5. Numerical examples** **10**
5.1. Ideal permanent magnet . . . 11
5.2. Non-linear permanent magnet . . . 11
5.3. Discussion . . . 12

**6. Conclusion** **12**

**A. Variational formulations** **13**

**B. Derivation of the magnetic polarization** **14**

**References** **14**

# 1. Introduction

Topology optimization (TO) is a fast-growing structural conception tool issued from mechanical engineering [1], which was introduced in the field of electromagnetic actuators with [2]. These methods aim to find $\Omega$ an admissible material distribution, which minimizes an objective function $f$:

$$\text{find} \quad \Omega^* = \arg\min f(\Omega). \tag{1}$$

Some methodologies try to solve this problem directly using heuristic algorithms such as particle swarm optimization [3], or genetic algorithms [4]; see [5] for a comparison. While they can handle a wide variety of problems easily and may be able to find their global optimum, heuristic approaches suffer from the high computing time due to the numerous variables $N > 10^3$ involved in TO [6]. Other works prefer faster optimization algorithms based on first-order derivatives. Among a wide variety of different approaches, such as the level set method [7] or the phase-field method [8] (see [9], [10] for exhaustive overviews), density-based methodologies are the most popular. They aim to solve a discretized and relaxed version of (1):

$$\text{find} \quad \boldsymbol{\rho}_{\text{opt}} = \arg \min_{\boldsymbol{\rho} \in [0,1]^N} f(\boldsymbol{\rho}), \tag{2}$$

where $\boldsymbol{\rho}$ is the vector containing $N$ optimization variables, called "densities", representing the filling level of each mesh element, similar to how pixels represent a geometry. A density value of 0 represents air, and a value of 1 represents a solid element such as steel, as shown in Fig. 1. The properties of


(a) Reference material distribution Ω

(b) Density-based representation of Ω

Figure 1: Density based geometry representation. Black elements ($\rho = 1$) represent solid material and white elements ($\rho = 0$) represent void.

materials, for example, Young modulus in mechanical engineering, or magnetic permeability in electrical engineering, can then be continuously interpolated with respect to the optimization variables $\boldsymbol{\rho}$. So, first-order derivatives can be computed efficiently with the Adjoint Variable Method (AVM) [9] in order to then use fast optimization algorithms based on gradient descent. However, the relaxed optimization problem (2) introduces the possibility of "gray materials", associated with a density $\rho$ between 0 and 1. They may be interpreted as a mixture between solid material and void, organized as micro-structures in homogenization methods such as [11].

There is some freedom in the material interpolation function. Concerning magnetic actuators, two trends exist in the literature. The magnetic permeability $\mu = |\boldsymbol{b}|/|\boldsymbol{h}|$ can be considered as the reference variable to interpolate, as in the seminal article [2]. A common interpolation, used in **jung2021**, [12]–[14], which mimics the SIMP scheme in mechanical engineering [15], is the following:

$$\mu(\rho, |\boldsymbol{b}|) = \mu_0 + (\mu_{\text{steel}}(|\boldsymbol{b}|) - \mu_0)\rho^p. \tag{3}$$

The other possibility is to interpolate, in a similar manner, the magnetic reluctivity $\nu = 1/\mu$. It was introduced by [16] and is used in numerous papers such as [17]–[22].

As they do not have a proper physical interpretation in general, intermediate materials should be eliminated, with penalization schemes [23] or filtering [24]. To model linear hard-magnetic materials, an additional optimization variable to model the remanence should be considered as in [21]. However, this formalism seems inadequate to model non-linear Permanent Magnets (PM). To address this issue, this work proposes to interpolate the magnetic polarization $\boldsymbol{m}$, which is the common underlying magnetic property of both soft magnetic materials, such as steel, and hard magnetic materials, such as PM. In addition, this interpolation naturally models the non-linearity of PM, which is necessary to take into account the demagnetization of PM, previously only considered in analytical or parametric optimizations [25]–[27].

This new interpolation is first explained and compared to the other classical $\mu$ and $\nu$ interpolations. It is then applied, as an example, to the case of the Multi-Material Topology Optimization (MMTO) of a Permanent Magnet Synchronous Machine (PMSM) rotor. To do so, its numerical implementation is given with respect to the materials' behavior laws and the optimization framework is detailed. Next, the results are presented and analyzed for ideal and non-ideal magnets, highlighting the effect of the non-linearity. Finally, the conclusion draws some perspectives on this work.

## 2. Physical analysis of the interpolations

Macroscopic magnetostatics is entirely described by Maxwell's equations and material behavioral laws, which can be formulated following two different conventions [28]:

$$\text{Kennelly convention:} \quad \boldsymbol{h} = \frac{1}{\mu_0}(\boldsymbol{b} - \boldsymbol{m}_b(\boldsymbol{b})), \tag{4a}$$

$$\text{Sommerfeld convention:} \quad \boldsymbol{b} = \mu_0(\boldsymbol{h} + \boldsymbol{m}_h(\boldsymbol{h})), \tag{4b}$$

with $\boldsymbol{b}$ the magnetic flux density, $\boldsymbol{h}$ the magnetic field, $\mu_0 = 4\pi \times 10^{-7}$H/m the void permeability, $\boldsymbol{m}_h$ the magnetization, and $\boldsymbol{m}_b = \mu_0 \boldsymbol{m}_h$ the magnetic polarization. Note that $\boldsymbol{m}_b = \mu_0 \boldsymbol{m}_h$. We recall the expression of the magnetic permeability $\mu = |\boldsymbol{b}|/|\boldsymbol{h}|$ and reluctivity $\nu = |\boldsymbol{h}|/|\boldsymbol{b}|$ for isotropic materials. We denote the norm of the vector as $b = |\boldsymbol{b}|$, $h = |\boldsymbol{h}|$ and $m = |\boldsymbol{m}|$. The following linear interpolations are considered for $M$ different materials:

$$\nu - \text{interpolation:} \quad \tilde{\nu}(b) = \nu_0 + \sum_{i=1}^{M} \rho_i (\nu_i(b) - \nu_0), \tag{5a}$$

$$\mu - \text{interpolation:} \quad \tilde{\mu}(b) = \mu_0 + \sum_{i=1}^{M} \rho_i (\mu_i(b) - \mu_0), \tag{5b}$$

$$\boldsymbol{m} - \text{interpolation:} \quad \tilde{\boldsymbol{m}}(\boldsymbol{b}) = \sum_{i=1}^{M} \rho_i \boldsymbol{m}_i(\boldsymbol{b}), \tag{5c}$$

where $\rho_i$ is the optimization variable associated with material $i$. We assume that $\{\rho_i\}_{1 \leq i \leq M}$ partitions the unit:

$$\sum_{i=1}^{M} \rho_i = 1. \tag{6}$$

At macroscopic scale, Ampere's theorem reads:

$$\oint_{\Gamma} \boldsymbol{h}.\mathrm{d}\boldsymbol{l} = I \tag{7}$$

where $\Gamma$ is a closed path oriented along the flux line of a macroscopic solenoid represented in Fig. 2, which embraces a current $I$. Equation (7) helps to interpret the different interpolations at a smaller scale in a mesoscopic Representative Volume Element (RVE). In the numerical implementation detailed in section 3, the RVE is a mesh element.

## 2.1. Serial assembly - $\nu$ interpolation

Let us define the average magnetic field on the RVE by $\langle h \rangle = \frac{1}{L} \int_0^L \boldsymbol{h}.\mathrm{d}\boldsymbol{l}$, with $L$ the length of the RVE. Then, using the classical behavior law $h = \nu b$, the partition of unity (6), the Ampère's theorem (7) and the non-divergence of the flux density which induces a constant $b$ in an RVE containing a serial assembly of materials, we obtain:

$$\langle h \rangle = \sum_{i=1}^{M} \frac{l_i}{L} \nu_i(b) b = \underbrace{\left( \nu_0 + \sum_{i=1}^{M} \frac{l_i}{L} (\nu_i(b) - \nu_0) \right)}_{\tilde{\nu} \text{ from (5a)}} b, \tag{8}$$

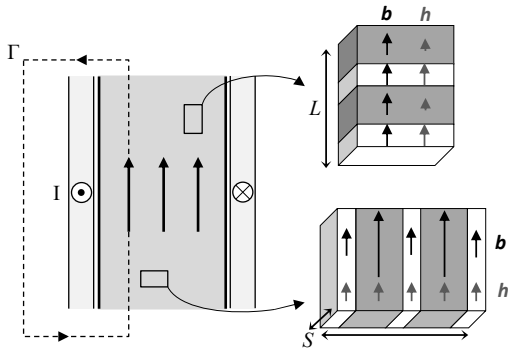


Figure 2: Illustration of the magnetic situation with a serial and a parallel RVE.

with $l_i$ the elementary length of material $i$. Equation (8) can be directly identified with Equation (5a), the optimization variable $\rho_i$ playing the role of lineic fraction $l_i/L$ of materials $i$. Therefore, linear $\nu$-interpolation can be identified with a serial assembly of materials along the flux lines. This interpolation is suitable when $b$ is the degree of freedom of the behavior law, *i.e.* when expressed in the Kennelly convention (See Equation (4a)). This is the case of the majority of finite element implementations, which are based on the "primal" vector potential $\boldsymbol{a}$; the associated magnetic behavior is shown in Fig. 3a. However, there is no indication that such an interpolation has a physical meaning when it is based on the magnetic field $h$ as in Fig. 3b.

## 2.2. Parallel assembly - $\mu$ interpolation

Let us define the average flux density $\langle b \rangle = \frac{1}{S}\iint_S \boldsymbol{b}.\mathrm{d}\boldsymbol{s}$, with $S$ the section of the RVE. Equation (7) gives the exact and constant magnetic field $h = I/L$ within all the parallel assembly RVE. Then, the average $\langle b \rangle$ can be computed by using (6) and the traditional material behavior law $b = \mu h$ to obtain:

$$\langle b \rangle = \sum_{i=1}^{M} \frac{s_i}{S}\mu_i(h)h = \underbrace{\left(\mu_0 + \sum_{i=1}^{M}\frac{s_i}{S}(\mu_i(h) - \mu_0)\right)}_{\tilde{\mu}(h)} h, \tag{9}$$

with $s_i$ the elementary section of material $i$. Note that (9) cannot be directly identified with (5b), as $\tilde{\mu}(h)$ depends on $h$ and not on $b$. Therefore, (9) makes sense as a parallel assembly along the flux lines only in the Sommerfeld convention (4b), where the optimization variable $\rho_i$ plays the role of surface fraction $s_i/S$ of material $i$. While the Sommerfeld convention is typically used in physics, it is rarely used in numerical implementation, where it is known as the dual formulation [29]: this magnetic behavior is plotted in Fig. 4b. Consequently, there is no simple physical interpretation of Equation (5b) which depends on $b$, or even no physical interpretation at all. Indeed, Fig. 4a shows that intermediate materials may have a differential permeability $\frac{\partial b}{\partial h}$ lower than $\mu_0$, which seems impossible.

## 2.3. $m$-interpolation

In fact, both Equations (8) and (9) can be rewritten to be identified with the unique physical quantity $m$ – formulated either in Sommerfeld or in Kennelly convention:

- In a serial assembly, we obtain with (4a) and (7):

$$\langle h \rangle = \frac{1}{\mu_0}\left(b - \underbrace{\sum_{i=1}^{M}\frac{l_i}{L}m_{b_i}(b)}_{Eq.\ (5c)\ -\ \text{Kennelly}}\right). \tag{10}$$

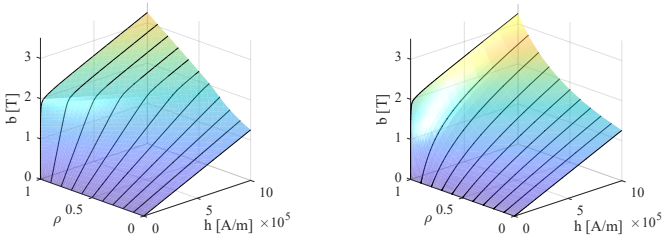


(a) Behavior law with $b$ dependance (serial assembly).

(b) Behavior law with $h$ dependance (no simple physical interpretation).

Figure 3: BH curves of intermediate materials for linear $\nu$-interpolation.

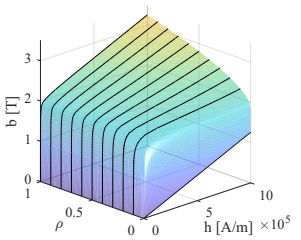


(a) Behavior law with $b$ dependance (no simple physical interpretation).

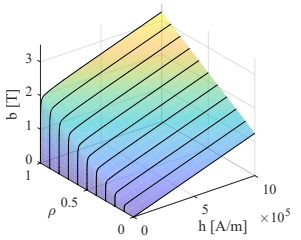


(b) Behavior law with $h$ dependance (parallel assembly).

Figure 4: BH curves of intermediate materials for linear $\mu$-interpolation.

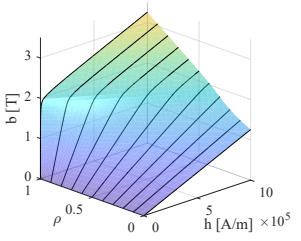


(a) Behavior law with $b$ dependance (serial assembly).

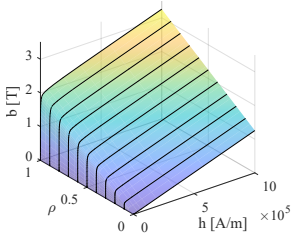


(b) Behavior law with $h$ dependance (parallel assembly).

Figure 5: BH curves of intermediate materials for linear $m$-interpolation.

- In a parallel assembly, we obtain with (4b) and (7):

$$\langle b \rangle = \mu_0 \Bigg( h + \underbrace{\sum_{i=1}^{M} \frac{s_i}{S} m_{h_i}(h)}_{Eq.\ (5c)\ -\ \text{Sommerfeld}} \Bigg). \tag{11}$$

Note that $m_b$ and $m_h$ represent the same physical quantity with a $\mu_0$ factor. Therefore $m$-interpolation is suited in both convention and the associated numerical formulations, as shown in Fig. 5.

## 2.4. Discussion

As shown in the previous sections, $\boldsymbol{m}$ seems to be the natural material property for interpolating magnetostatics topology optimization problems.

However, this interpolation is vectorial by nature – as in Equations (4a) and (4b) – so its numerical implementation detailed in Section 3 is more tedious than $\mu$ or $\nu$ interpolations. In addition, equivalent interpolations can be achieved with $\nu$ following the Kennelly convention (classical finite element formulation) or $\mu$ following the Sommerfeld convention (dual formulation) when dealing with soft magnetic materials only, as shown in Sec. 2.

In fact, the practical usefulness of vectorial $\boldsymbol{m}$-interpolation becomes apparent when dealing with a mixture of hard magnetic materials and non-linear soft magnetic materials. The usual material laws

- $\boldsymbol{h} = \nu \boldsymbol{b}$ for soft materials, where $\nu = \frac{h}{b}$, and
- $\boldsymbol{h} = \nu_0(\boldsymbol{b} - \boldsymbol{m}_b)$ for hard materials, where $\nu = \frac{\Delta h}{\Delta b}$,

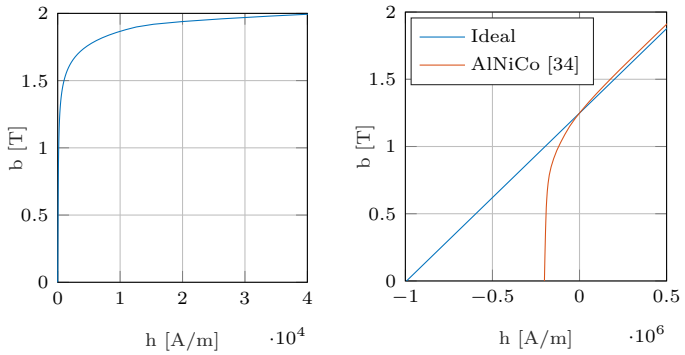


(a) FeSi anhysteretic BH curve (b) BH curves of PM.

Figure 6: BH curves of soft and hard magnetic materials.

are simplifications of (4a) that are valid under the assumptions $\boldsymbol{m}_b = 0$ when $\boldsymbol{b} = 0$ for soft materials, and $\boldsymbol{m}_b$ is a constant for hard materials. Such conditions are in contradiction of each other, which makes the interpretation of intermediate materials obtained by $\nu$-interpolation difficult to interpret. Indeed, the interpretation of the coefficient $\nu$ itself differs for hard and soft materials. Similarly, a non-linear permanent magnet behaves like a mixture of ideal soft and ideal hard materials, and its behavior is well-described through its magnetic polarization model.

Therefore, the $\boldsymbol{m}$ - interpolation handles general magnetic behaviors similar to gradient-free topology optimization, where an independent black-box magnetic solver is often used without the need of intermediate materials. In contrast, in density-based topology optimization, the user must consistently define the material models of the real and intermediate materials.

# 3. Numerical implementation

## 3.1. Magnetic materials behavior

The anhysteretic magnetic polarization of anhysteretic soft magnetic materials such as FeSi can be fully determined by its scalar BH curve, such as in Fig. 6a. Assuming its reciprocal function $h(b)$ is known, $\boldsymbol{m}$ reads:

$$\boldsymbol{m}_{FeSi}(\boldsymbol{b}) = m_{FeSi}(b) \cdot \boldsymbol{u}_b, \tag{12}$$

where $m_{FeSi}(b) = b - \mu_0 h(b)$ is deduced from (4a) and the BH curve, $\boldsymbol{u}_b = \frac{\boldsymbol{b}}{b}$ a unitary vector oriented along the induction. Concerning ideal hard magnetic materials, $\boldsymbol{m}$ is a constant. However, the magnetic polarization of realistic hard materials depends on the norm of $b$ and its direction. It requires a vector hysteresis model such as [30], [31]. In addition, irreversibility and hysteresis models may be considered but increase the computation time significantly, which is a severe issue for topology optimization.

Therefore, the irreversibility of magnetic materials is not taken into account in this work, and the following simplified magnetic model of PM is considered to save computing time :

$$\boldsymbol{m}_{pm}(\boldsymbol{b}) = m_{pm}(\boldsymbol{b}) \cdot \boldsymbol{u}_{pm}, \tag{13}$$

where $\boldsymbol{m}_{pm}$ is the magnetic polarization of PM, $\boldsymbol{u}_{pm}$ is the unitary vector indicating its fixed direction, and $m_{pm}(\boldsymbol{b}) = \boldsymbol{b} \cdot \boldsymbol{u}_{pm} - \mu_0 h(\boldsymbol{b} \cdot \boldsymbol{u}_{pm})$ is its norm. This model requires the magnet's $h(b)$ behavior along its d-axis, such as in Fig. 6b. More elaborated models are possible such as vectorized Jiles-Atherton [32].

### 3.2. 2D magnetostatics with m-formulation

Using the general behavior law in the Kennelly convention (4a), Maxwell's equations give the following magnetostatics equation:

$$\nabla \times (\nu \nabla \times \boldsymbol{a}) = \mu_0 \boldsymbol{j} + \nabla \times \boldsymbol{m}(\boldsymbol{b}), \tag{14}$$

where $\boldsymbol{a}$ is the magnetic vector potential verifying $\nabla \times \boldsymbol{a} = \boldsymbol{b}$, and $\boldsymbol{j}$ is the current density. Magnetic polarization is not limited to a permanent magnet but to all magnetic materials, including soft magnetic materials, and is zero in non-magnetic materials. In 2D problems where $\boldsymbol{a} = [0 \quad 0 \quad a_z]$, $\boldsymbol{j} = [0 \quad 0 \quad j_z]$ and $\boldsymbol{m} = [m_x \quad m_y \quad 0]$, (14) becomes:

$$-\nabla \cdot (\nu \nabla a_z) = \mu_0 j_z + \nabla \cdot \big(m_y(\boldsymbol{b}) - m_x(\boldsymbol{b})\big). \tag{15}$$

This equation can be discretized with the finite element method to obtain the non-linear system (16). After discretization, the finite element system can be assembled and reads:

$$\mathbf{K}\boldsymbol{a} = \mathbf{s}(\boldsymbol{a}, \boldsymbol{\rho}), \tag{16}$$

which is solved with a Newton-Raphson scheme. The associated solver was implemented in Matlab and validated with GetDp [34]. More details are given in appendixes A and B.

## 4. Optimization formalism

This article considers the Multi-Material Topology Optimization (MMTO) of a Permanent Magnet Synchronous Machine (PMSM) rotor. Three different materials are considered:

- Anhysteretic steel (standard FeSi);
- PM with a fixed orientation of 15° for the sake of simplicity, which may restrict the possible solutions - note that it is possible to include the magnetization direction in the optimization problem [11], [21]. However, the PM can be non-linear;
- Air.

### 4.1. Multi-material interpolation

To use a density-based method, it is necessary to define an interpolation between the magnetic polarization of the different materials. To do so, two optimization variables contained in a square $\rho_1, \rho_2 \in [-1, 1]^2$ are used per mesh element. A material is attributed to each vertex of this square, so the interpolated $\tilde{\boldsymbol{m}}$ reads:

$$\begin{aligned}\tilde{\boldsymbol{m}}(\rho_1, \rho_2, \boldsymbol{b}) = \omega_{pm}(\rho_1, \rho_2)\boldsymbol{m}_{pm}(\boldsymbol{b}) + \\ \omega_{FeSi}(\rho_1, \rho_2)\boldsymbol{m}_{FeSi}(\boldsymbol{b}),\end{aligned} \tag{17}$$

with $\boldsymbol{m}_{pm}$ the polarization of the permanent magnet, $\boldsymbol{m}_{FeSi}$ the polarization of the steel, $\omega_{pm}$ and $\omega_{FeSi}$ the weight functions, associated to permanent magnet and steel, respectively. The weight functions, also used in [35], [36], are plotted in Fig. 7, and read:

$$\omega_{PM}(\rho_1, \rho_2) = \frac{1}{4}(\rho_1 + 1)(1 - \rho_2), \tag{18a}$$

$$\omega_{FeSi}(\rho_1, \rho_2) = \frac{1}{4}(1 - \rho_1)(\rho_2 + 1). \tag{18b}$$

Note that, $\boldsymbol{m}$-interpolation (17) can handle any magnetic material without additional variables, as long as a vector model is available for $\boldsymbol{m}(\boldsymbol{b})$. This is not the case with $\mu$- or $\nu$- interpolations that

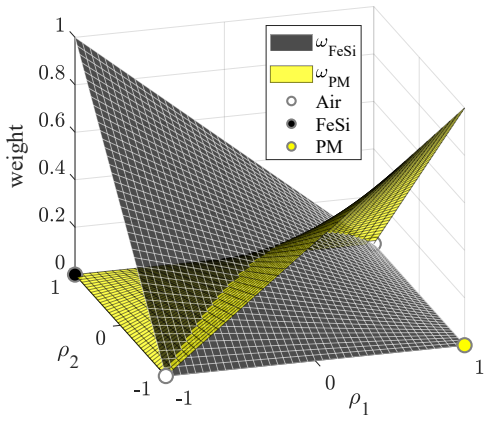


Figure 7: Weight functions $\omega_{FeSi}$ and $\omega_{PM}$ with material placement.

require the addition of the PM remanence, for example, which is already included within the magnetic polarization model.

Since the optimized designs do not contain intermediate materials, there is no need to introduce an exponent $p$ as in Eq. (3). This is similar to $\nu$- interpolation optimizations which are self-penalized [16], [20], and corresponds to the same serial-assembly interpretation as $\boldsymbol{m}$-interpolation in vector-potential magnetostatics formulation (see Sec. 2).

## 4.2. Objective function

The aim of this optimization is to maximize the average torque. From Maxwell's stress tensor $\Sigma$, the torque $\boldsymbol{t}$ of a rotating machine can be written as a line integral within the airgap [37]:

$$\boldsymbol{t} = L \oint_{\gamma} \boldsymbol{r} \times \Sigma \boldsymbol{n} \, \mathrm{d}\gamma, \tag{19}$$

where $L$ is the axial length of the machine, $\boldsymbol{r}$ the position vector, $\boldsymbol{n}$ the outer normal vector from the path $\gamma$. $\Sigma$ can be reduced to its magnetic component, which reads:

$$\Sigma_{ij} = \frac{1}{\mu_0} \left( b_i b_j - \frac{|\boldsymbol{b}|^2}{2} \delta_{ij} \right), \tag{20}$$

where $\delta_{ij}$ is the Kronecker delta. Equation (19) can be rewritten as a surface integral within the airgap's surface $S_e$, so the following expression is used:

$$\boldsymbol{t} = \frac{2\pi L}{S_e} \iint_{S_e} \boldsymbol{r} \times \Sigma \boldsymbol{r} \, \mathrm{d}s. \tag{21}$$

Only the $z$ component of $\boldsymbol{t}$ is interesting in 2D. This expression depends explicitly on the magnetic flux density $\boldsymbol{b}$, but not on the design variables $\boldsymbol{\rho}$. The design variables and the physical state (also called the *direct state*) are linked implicitly by the non-linear physical system (16). Therefore, the Adjoint Variable Method (AVM) [9] is necessary to compute the problem sensitivities.

## 4.3. Optimization problem

A volume constraint is set to avoid the rotor being filled entirely with the permanent magnet. The maximal volume of the permanent magnet is arbitrarily set to 10% of the total rotor volume. The optimization problem can now be formulated under the standard form:

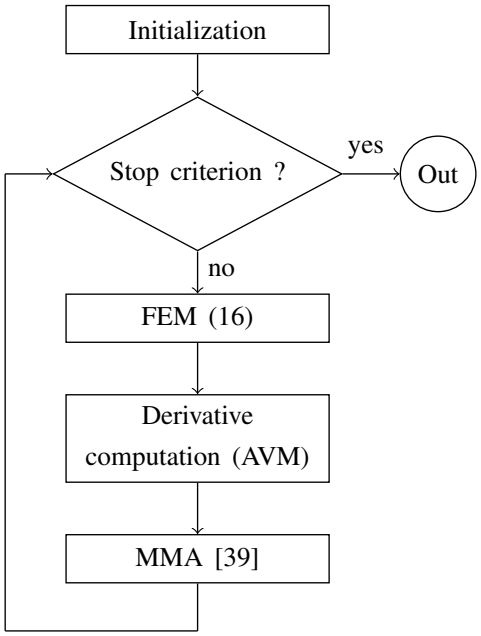


Figure 8: Flowchart of the optimization algorithm.

$$\begin{aligned} \text{find} \quad & \boldsymbol{\rho}_{opt} = \arg\max \langle \boldsymbol{t}.\boldsymbol{e}_z \rangle, \\ \text{subject to} \quad & \iint_{\mathcal{R}} \omega_{10} \mathrm{d}s / \iint_{\mathcal{R}} 1 \mathrm{d}s \leq 10\%, \end{aligned} \tag{22}$$

where $\mathcal{R}$ is the optimization zone, *i.e.*, the rotor of the machine. The Method of Moving Asymptote [38] (MMA) is used to perform the optimization. Neither filtering nor post-processing. The algorithm stops after 500 iterations. The optimization flowchart is given in Fig. 8. The average computing times per iteration were about 8.4 s for the FEM, 1.0 s for the AVM and 0.1 s for MMA.

## 5. Numerical examples

The MMTO problem given in Equation (22) is applied to the rotor optimization of a single PMSM pole. The mesh generated by GMSH [39] contains 5890 nodes and 11331 first-order triangles, with 3441 located in the rotor leading to a total of 6882 design variables. A sliding band technique [40] emulates the rotation without remeshing. The torque is averaged on 60 angular positions. The stator is fixed, and the current feedings of the three phases read:

$$\begin{cases} J_{A+}(\theta_e) = J\cos\left(\theta_e + \phi\right) \\ J_{C-}(\theta_e) = J\cos\left(\theta_e - \frac{\pi}{3} + \phi\right) \\ J_{B+}(\theta_e) = J\cos\left(\theta_e - \frac{2\pi}{3} + \phi\right), \end{cases} \tag{23}$$

where $J$ is the current density amplitude set to $10\,\mathrm{A/mm^2}$, $\theta_e$ the electric angle, and $\phi$ the load angle, which is an electrical rotation between the initial position of the rotor and the flux created by the stator. As only one orientation of permanent magnet is available in this optimization, $\phi = 240°$ is chosen to place it in the center of the rotor pole. The optimization is performed with two different types of PM:

- Ideal permanent magnet with a constant magnetic polarization
- AlNiCo magnet

Their remanent flux densities are set to 1.25 T, representing the nominal remanence of AlNiCo magnets. Only their coercive fields are different; see Fig. 6b for their BH curves. The initial situation for both optimizations is homogeneous to demonstrate the ability of the methodology to find performing designs without any initial information and is given in Fig. 9. To avoid starting on the FeSi - PM diagonal representing a magnetic polarization saddle line, all the optimization variables are initialized to 0.1 and not in the center of the domain. A simple spatial mean-filter procedure [41] is applied to limit the geometry artifacts. The radius of the filter decreases from 3 mm to 0 mm every 50 iterations to obtain sharp interfaces in the final design. Other filtering schemes or post-processing [24] may be used to remove the remaining geometric artifacts.

## 5.1. Ideal permanent magnet

First, the optimization uses an ideal permanent magnet with a constant magnetic polarization as a candidate material. The final result is shown in Fig. 10. A Surface Permanent Magnet Synchronous Machine (SPMSM) rotor is obtained, in agreement with the results found in [42]. The optimization evolution and result are shown in Fig. 10. The final torque is 2836 Nm/m, and the PM volume constraint is respected.

We note that the optimized permanent magnet area is thin. Therefore, there is a risk of demagnetization in a practical situation. Indeed, the high demagnetizing field within the PM shown in Fig. 11a locally reduces the flux density shown in Fig. 11b, and may cause demagnetization in practical situations.

This result highlights the importance of considering the non-linearity of the magnetic behavior during optimization, especially when using semi-hard magnetic materials such as AlNiCo.

## 5.2. Non-linear permanent magnet

The demagnetization can be partially taken into account in the optimization by considering the upper BH curve of an AlNiCo. This material was chosen due to its relatively low coercivity compared to other PM types. Only the non-linearity of the BH curve is considered and the recoil lines follow the hysteresis curve, which is not the case in real demagnetization, see [43]. However, this simplified model is enough to change significantly the obtained design shown in Fig. 12a from the ideal PM case. The torque plotted in Fig. 12b is degraded by 19 % and reaches 2293 Nm/m, while the PM volume constraint is still respected.

Note that the position of the PM has changed to avoid the high demagnetizing field located at the bottom of Fig. 11a and its width has increased in the zone where the demagnetizing field is important. The demagnetizing field is now very limited in the PM and is more located in the air, as shown in Fig. 13a and Fig. 13b.

The non-linear behavior of the PM seems to induce more artifacts, such as small isolated structures in the optimized design, shown in Fig. 12a. Additional filtering or regularization schemes may be necessary for a more general case.

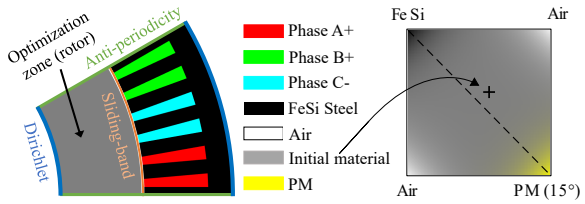


Figure 9: Initial situation corresponding to 6 pole pairs, and intermediate materials' colorscale.

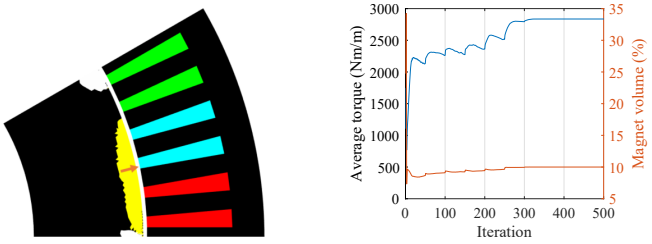


(a) Optimized design (b) Torque and PM volume

Figure 10: Results of the optimization with an ideal PM.

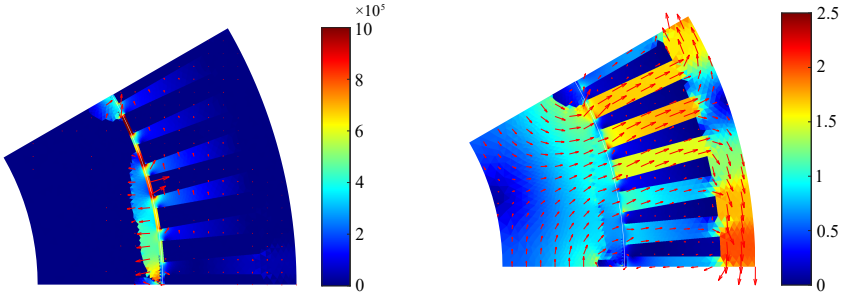

(a) Magnetic field (A/m) (b) Flux density (T)

Figure 11: Magnetic field and flux density of the optimized design with an ideal PM.

## 5.3. Discussion

The instant torques are plotted in Fig. 14 and compared to a reference BMWi3 reference design adapted from [44] with ideal PM, the same rotor diameter and current feedings.Additional information such as the ripple $r = \frac{\max(T)-\min(T)}{\langle T \rangle}$ and the PM volume are given in Table 1.

Table 1: Performance of the designs.

| | Ref. design (ideal PM) | Optim. design ideal PM | Optim. design AlNiCo |
|---|---|---|---|
| Avg. torque | 2404 Nm/m | 2836 Nm/m | 2293 Nm/m |
| Ripple | 29% | 22% | 34% |
| PM volume | 20% | 10% | 10% |

The optimized design with the ideal PM has a higher average torque than the reference one with a lower PM volume, which validates the topology optimization methodology. However, the higher torque may be explained by the lack of mechanical constraint, leading to magnetic short circuits. Note that the decrease of torque ripple was not expected in the optimized design with ideal PM. The torque ripple could be reduced even more by adding it explicitly as an objective function [19].

Moreover, it was recently shown in [45], [46] that the electric angle $\phi$ should be controlled during the optimization in the presence of PM to obtain better performance. Here, $\phi$ is fixed to compare the two final structures, which otherwise would reach different optimal $\phi$.

# 6. Conclusion

This article presents the magnetic polarization interpolation applied to the MMTO of a PMSM rotor. In its physical interpretation and applications, the $\boldsymbol{m}$-interpolation is more general than $\mu$- or $\nu$- interpolations. Indeed, it allows the consideration the non-linearity of the PM within the optimization process.

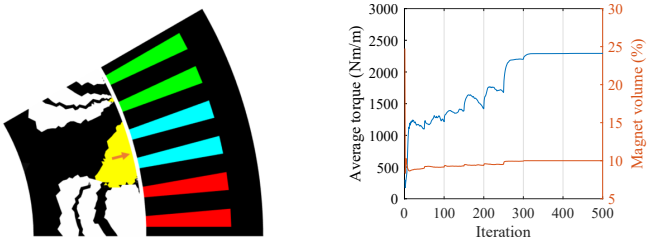


(a) Optimized design (b) Torque and PM volume

Figure 12: Magnetic field and flux density with a non-linear PM.

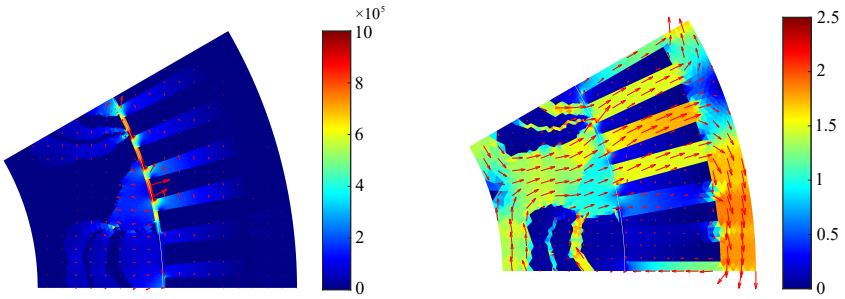


(a) Magnetic field (A/m) (b) Flux density (T)

Figure 13: Magnetic field and flux density with AlNiCo PM.

Numerical examples show that the optimized design could be significantly modified by considering the non-linearity of the PM behavior, even with a simplified model.

This methodology can be extended to address dynamic demagnetization with more realistic vector hysteresis models such as [32]. Potential applications include innovative electrical actuators such as memory machines [47], which are beyond the current state of the art in topology optimization. Other perspectives include additional physics, such as thermals to obtain a realistic PM demagnetization model, or mechanics to ensure the rotor's strength.

## A. Variational formulations

The finite element discretization (16) uses the weak form of Eq. (15) on the computational domain $\mathcal{D}$ composed by the rotor, the stator, and the airgap. The weak form of its residual reads:

$$\forall (a, a^*) \in H_0^1(\mathcal{D}) \times H_0^1(\mathcal{D}), \quad r(a, a^*) = \int_{\mathcal{D}} \nabla a^* \cdot \nabla a - \int_{\mathcal{D}} a^* \mu_0 j_z + \int_{\mathcal{D}} \nabla a^* \cdot R_{-\pi/2}\, \boldsymbol{m}(\boldsymbol{b}), \tag{24}$$

with $R_{-\pi/2} = \begin{bmatrix} 0 & 1 \\ -1 & 0 \end{bmatrix}$ a rotation operator. Eq. (24) can be discretized with the FEM to obtain (16). To solve it, the Newton method comes from the first-order expansion of the residual:

$$r(a + \delta a, a^*) \simeq r(a, a^*) + \mathrm{d}_a r(\delta a, a^*) = 0, \tag{25}$$

where

$$\mathrm{d}_a r(\delta a, a^*) = \int_{\mathcal{D}} \nabla a^* \cdot \nabla \delta a + \int_{\mathcal{D}} \nabla a^* \cdot R_{-\pi/2}\, \mathrm{d}_{\boldsymbol{b}} \boldsymbol{m}\, \mathrm{d}_a \delta \boldsymbol{b}, \tag{26}$$

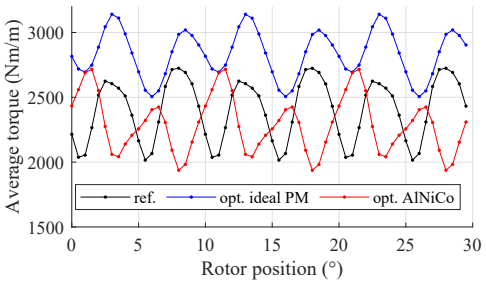


Figure 14: Instant torques associated with the designs obtained with ideal PM and AlNiCo compared to the reference.

and $\delta a = a_{k+1} - a_k$. Since $\delta \boldsymbol{b} = R_{-\pi/2} \nabla \delta a$, we should assemble and solve iteratively until convergence:

$$\int_{\mathcal{D}} \nabla a^* \cdot (I_d + R_{-\pi/2}\ \mathrm{d}_{\boldsymbol{b}}\boldsymbol{m}(\boldsymbol{b}_k)\ R_{-\pi/2}) \nabla a_{k+1} = \int_{\mathcal{D}} \nabla a^* \cdot (I_d + R_{-\pi/2}\ \mathrm{d}_{\boldsymbol{b}}\boldsymbol{m}(\boldsymbol{b}_k)\ R_{-\pi/2}) \nabla a_k - r(a_k, a^*), \quad (27)$$

$I_d$ being the identity matrix.

## B. Derivation of the magnetic polarization

The term $\mathrm{d}_{\boldsymbol{b}}\boldsymbol{m}(\boldsymbol{b})$ is symmetric and can be explicitly calculated:

- for soft magnetic material, Eq.(12) gives:

$$\mathrm{d}_b \boldsymbol{m}_{FeSi} = \frac{m'_{FeSi}(|\boldsymbol{b}|)}{|\boldsymbol{b}|^2} \cdot \boldsymbol{b} \otimes \boldsymbol{b} + \frac{m_{FeSi}(|\boldsymbol{b}|)}{|\boldsymbol{b}|^3} \cdot \begin{bmatrix} b_y^2 & -b_x b_y \\ -b_x b_y & b_x^2 \end{bmatrix} \quad (28)$$

- for hard magnetic material, Eq.(13) gives:

$$\mathrm{d}_b \boldsymbol{m}_{pm} = m'_{pm}(\boldsymbol{b} \cdot \boldsymbol{u}_m) \cdot \boldsymbol{u}_{\boldsymbol{m}} \otimes \boldsymbol{u}_{\boldsymbol{m}} \quad (29)$$

## Acknowledgment

The authors would like to thank the Moulon Mesocentre of Paris-Saclay University team for the calculations.

## References

[1] M. P. Bendsøe and N. Kikuchi, "Generating optimal topologies in structural design using a homogenization method," *Computer Methods in Applied Mechanics and Engineering*, vol. 71, no. 2, pp. 197–224, 1988. DOI: 10.1016/0045-7825(88)90086-2 (cit. on p. 2).

[2] D. N. Dyck and D. A. Lowther, "Automated design of magnetic devices by optimizing material distribution," *IEEE Transactions on Magnetics*, vol. 32, no. 3 PART 2, pp. 1188–1192, 1996. DOI: 10.1109/20.497456 (cit. on pp. 2–3).

[3] C. Ma and L. Qu, "Multiobjective Optimization of Switched Reluctance Motors Based on Design of Experiments and Particle Swarm Optimization," *IEEE Transactions on Energy Conversion*, vol. 30, no. 3, pp. 1144–1153, 2015 (cit. on p. 2).

[4] C. H. Im, H. K. Jung, and Y. J. Kim, "Hybrid Genetic Algorithm for Electromagnetic Topology Optimization," *IEEE Transactions on Magnetics*, vol. 39, no. 5 I, pp. 2163–2169, 2003. DOI: 10.1109/TMAG.2003.817094 (cit. on p. 2).

[5] F. Cupertino, G. Pellegrino, and C. Gerada, "Design of synchronous reluctance motors with multiobjective optimization algorithms," *IEEE Transactions on Industry Applications*, vol. 50, no. 6, pp. 3617–3627, 2014. DOI: 10.1109/TIA.2014.2312540 (cit. on p. 2).

[6] O. Sigmund, "On the usefulness of non-gradient approaches in topology optimization," *Structural and Multidisciplinary Optimization*, vol. 43, no. 5, pp. 589–596, 2011. DOI: 10.1007/s00158-011-0638-7 (cit. on p. 2).

[7] P. Gangl, U. Langer, A. Laurain, *et al.*, "Shape optimization of an electric motor subject to nonlinear magnetostatics," *SIAM Journal on Scientific Computing*, vol. 37, no. 6, B1002–B1025, 2015. DOI: 10.1137/15100477X (cit. on p. 2).

[8] J. S. Choi, K. Izui, S. Nishiwaki, *et al.*, "Topology optimization of the stator for minimizing cogging torque of IPM motors," *IEEE Transactions on Magnetics*, vol. 47, no. 10, pp. 3024–3027, 2011. DOI: 10.1109/TMAG.2011.2158572 (cit. on p. 2).

[9] F. Campelo, J. A. Ramírez, and H. Igarashi, *A survey of topology optimization in electromagnetics : considerations and current trends*, 2010 (cit. on pp. 2–3, 9).

[10] F. Lucchini, R. Torchio, V. Cirimele, *et al.*, "Topology Optimization for Electromagnetics: A Survey," *IEEE Access*, vol. 10, no. August, pp. 98 593–98 611, 2022. DOI: 10.1109/access.2022.3206368 (cit. on p. 2).

[11] J. Lee, T. Nomura, and E. M. Dede, "Topology optimization of magnetic composite microstructures for electropermanent magnet," *Journal of Magnetism and Magnetic Materials*, vol. 503, p. 166 596, Feb. 2020. DOI: 10.1016/j.jmmm.2020.166596 (cit. on pp. 3, 8).

[12] J.-K. Byun, S.-Y. Hahn, and I.-H. Park, "Topology optimization of electrical devices using mutual energy and sensitivity," *IEEE Transactions on Magnetics*, vol. 35, no. 5, pp. 3718–3720, Sep. 1999. DOI: 10.1109/20.800642 (cit. on p. 3).

[13] S. Wang, D. Youn, H. Moon, *et al.*, "Topology optimization of electromagnetic systems considering magnetization direction," *IEEE Transactions on Magnetics*, vol. 41, no. 5, pp. 1808–1811, 2005. DOI: 10.1109/TMAG.2005.846480 (cit. on p. 3).

[14] T. Labbé and B. Dehez, "Topology optimization method based on the maxwell stress tensor for the design of ferromagnetic parts in electromagnetic actuators," *IEEE Transactions on Magnetics*, vol. 47, no. 9, pp. 2188–2193, 2011. DOI: 10.1109/TMAG.2011.2138151 (cit. on p. 3).

[15] M. P. Bendsøe, "Optimal shape design as a material distribution problem," *Structural optimization*, vol. 1, no. 4, pp. 193–202, 1989. DOI: 10.1007/BF01650949 (cit. on p. 3).

[16] J. S. Choi and J. Yoo, "Structural optimization of ferromagnetic materials based on the magnetic reluctivity for magnetic field problems," *Computer Methods in Applied Mechanics and Engineering*, vol. 197, no. 49-50, pp. 4193–4206, 2008. DOI: 10.1016/j.cma.2008.04.019 (cit. on pp. 3, 9).

[17] J. Lee, J. H. Seo, and N. Kikuchi, "Topology optimization of switched reluctance motors for the desired torque profile," *Structural and Multidisciplinary Optimization*, vol. 42, no. 5, pp. 783–796, 2010. DOI: 10.1007/s00158-010-0547-1 (cit. on p. 3).

[18] J. Lee, E. M. Dede, and T. Nomura, "Simultaneous design optimization of permanent magnet, coils, and ferromagnetic material in actuators," *IEEE Transactions on Magnetics*, vol. 47, no. 12, pp. 4712–4716, 2011. DOI: 10.1109/TMAG.2011.2160870 (cit. on p. 3).

[19] E. Kuci, F. Henrotte, P. Duysinx, *et al.*, "Combination of topology optimization and Lie derivative-based shape optimization for electro-mechanical design," *Structural and Multidisciplinary Optimization*, vol. 59, no. 5, pp. 1723–1731, 2019. DOI: 10.1007/s00158-018-2157-2 (cit. on pp. 3, 12).

[20] P. Seebacher, M. Kaltenbacher, F. Wein, *et al.*, "A pseudo density topology optimization approach in nonlinear electromagnetism applied to a 3D actuator," *International Journal of Applied Electromagnetics and Mechanics*, vol. 65, no. 3, pp. 545–559, 2020. DOI: 10.3233/jae-201501 (cit. on pp. 3, 9).

[21] T. Gauthey, P. Gangl, and M. H. Hassan, "Multi-Material Topology Optimization with Continuous Magnetization Direction for motors design," in *International Conference on Electrical Machines 2022*, (Sep. 5–8, 2022), Valencia: IEEE, 2022 (cit. on pp. 3, 8).

[22] T. Cherrière, L. Laurent, S. Hlioui, *et al.*, "Topology optimization of asymmetric pmsm rotor," in *International Conference on Electrical Machines 2022*, (Sep. 5–8, 2022), Valencia: IEEE, 2022 (cit. on p. 3).

[23] M. P. Bendsøe and O. Sigmund, "Material interpolation schemes in topology optimization," *Archive of Applied Mechanics*, vol. 69, no. 9-10, pp. 635–654, 1999. DOI: 10.1007/s004190050248 (cit. on p. 3).

[24] O. Sigmund, "Morphology-based black and white filters for topology optimization," *Structural and Multidisciplinary Optimization*, vol. 33, no. 4-5, pp. 401–424, 2007. DOI: 10.1007/s00158-006-0087-x (cit. on pp. 3, 11).

[25] Z. Wan and I. Husain, "Design, analysis and prototyping of a flux switching transverse flux machine with ferrite magnets," *2017 IEEE Energy Conversion Congress and Exposition, ECCE 2017*, vol. 2017-Janua, pp. 1227–1233, 2017. DOI: 10.1109/ECCE.2017.8095929 (cit. on p. 3).

[26] D. Fan, L. Quan, X. Zhu, *et al.*, "Demagnetization investigation of a partitioned rotor flux switching machine with hybrid permanent magnet," *AIP Advances*, vol. 7, no. 5, pp. 1–8, 2017. DOI: 10.1063/1.4974975 (cit. on p. 3).

[27] Z. Sheng and D. Wang, "Design and analysis of a kind of rotor ironless high torque density machine using Alnico magnet," *IET Electric Power Applications*, vol. 14, no. 8, pp. 1396–1404, 2020. DOI: 10.1049/iet-epa.2019.0774 (cit. on p. 3).

[28] J. E. Coleman, "Conventions for Magnetic Quantities in SI," *American Journal of Physics*, vol. 41, no. 2, pp. 221–223, 1973. DOI: 10.1119/1.1987179 (cit. on p. 3).

[29] Z. Ren and N. Ida, "Derivation of various dual formulations in magnetostatics via error based energy approach," *IEEE Transactions on Magnetics*, vol. 35, no. 3 PART 1, pp. 1167–1170, 1999. DOI: 10.1109/20.767156 (cit. on p. 5).

[30] F. Preisach, "Über die magnetische nachwirkung," *Z. Physik*, vol. 94, pp. 277–302, 1935 (cit. on p. 7).

[31] E. C. Stoner and E. P. Wohlfarth, "A mechanism of magnetic hysteresis in heterogeneous alloys," *Philosophical Transactions of the Royal Society Ser. A*, vol. 240, 826 1948 (cit. on p. 7).

[32] G. Szymański and M. Waszak, "Vectorized Jiles-Atherton hysteresis model," *Physica B: Condensed Matter*, vol. 343, no. 1-4, pp. 26–29, 2004. DOI: 10.1016/j.physb.2003.08.048 (cit. on pp. 7, 13).

[33] Arnold® Magnetic Technologies. "Cast alnico permanent magnets brochure (alnico5)." (2003), [Online]. Available: https://www.arnoldmagnetics.com/wp-content/uploads/2017/10/Cast-Alnico-Permanent-Magnet-Brochure-101117.pdf (visited on 08/15/2022).

[34] P. Dular, C. Geuzaine, A. Genon, *et al.*, "An evolutive software environment for teaching finite element methods in electromagnetism," *IEEE Transactions on Magnetics*, vol. 35, no. 3, pp. 1682–1685, May 1999 (cit. on p. 8).

[35] Y. Jung and S. Min, "Material Interpolation in Multi-Material Topology Optimization for Magnetic Device Design," *IEEE Transactions on Magnetics*, vol. 55, no. 11, pp. 2019–2022, 2019. DOI: 10.1109/TMAG.2019.2929079 (cit. on p. 8).

[36] T. Cherrière, L. Laurent, S. Hlioui, *et al.*, "Multi-material topology optimization of a rotating electrical machine with a density-based method," *PAMM*, vol. 21, no. S1, e202100259, 2021. DOI: https://doi.org/10.1002/pamm.202100259 (cit. on p. 8).

[37] N. Sadowski, Y. Lefevre, M. Lajoie-Mazenc, *et al.*, "Finite Element Torque Calculation In Electrical Machines While Considering The Mouvement," *IEEE Transactions on Magnetics*, vol. 28, no. 2, pp. 1410–1413, 1992. DOI: 10.1109/20.123957 (cit. on p. 9).

[38] K. Svanberg, "The method of moving asymptotes—a new method for structural optimization," *International Journal for Numerical Methods in Engineering*, vol. 24, no. 2, pp. 359–373, 1987. DOI: 10.1002/nme.1620240207 (cit. on p. 10).

[39] C. Geuzaine and J. Remacle, "Gmsh: A 3-D finite element mesh generator with built-in pre- and post-processing facilities," *International Journal for Numerical Methods in Engineering*, vol. 79, no. 11, pp. 1309–1331, May 2009. DOI: 10.1002/nme.2579 (cit. on p. 10).

[40] X. Shi, Y. Le Menach, J. P. Ducreux, *et al.*, "Comparison of slip surface and moving band techniques for modelling movement in 3D with FEM," *COMPEL - The International Journal for Computation and Mathematics in Electrical and Electronic Engineering*, vol. 25, no. 1, pp. 17–30, 2006. DOI: 10.1108/03321640610634290 (cit. on p. 10).

[41] O. Sigmund and J. Petersson, "Numerical instabilities in topology optimization: A survey on procedures dealing with checkerboards, mesh-dependencies and local minima," *Structural Optimization*, vol. 16, no. 1, pp. 68–75, 1998. DOI: 10.1007/BF01214002 (cit. on p. 11).

[42] S. Park, J. Lee, and J. Lee, "Multi-material topology optimization of permanent magnet synchronous motors," *International Journal of Applied Electromagnetics and Mechanics*, vol. 67, no. 4, pp. 461–472, 2021. DOI: 10.3233/JAE-210062 (cit. on p. 11).

[43] S. Sjökvist and S. Eriksson, "Experimental verification of a simulation model for partial demagnetization of permanent magnets," *IEEE Transactions on Magnetics*, vol. 50, no. 12, pp. 1–5, 2014. DOI: 10.1109/TMAG.2014.2339795 (cit. on p. 11).

[44] D. Staton and J. Goss, "Open Source Electric Motor Models for Commercial EV & Hybrid Traction Motors," in *CWIEME*, Berlin, 2017, pp. 46–59 (cit. on p. 12).

[45] C. Lee and I. Gwun, "Multi-material topology optimization for the PMSMs under the consideration of the MTPA control," *Structural and Multidisciplinary Optimization*, pp. 1–11, 2022. DOI: 10.1007/s00158-022-03367-x (cit. on p. 12).

[46] T. Cherrière, L. Laurent, S. Hlioui, *et al.*, "Multi-material topology optimization using Wachspress interpolations for designing a 3 - phase electrical machine stator," *Structural and Multidisciplinary Optimization*, vol. 65, no. 12, p. 352, 2022. DOI: 10.1007/s00158-022-03460-1 (cit. on p. 12).

[47] J. Huang, X. Wang, and Z. Sun, "Variable flux memory motors: A review," *IEEE Transportation Electrification Conference and Expo, ITEC Asia-Pacific 2014 - Conference Proceedings*, pp. 1–6, 2014. DOI: 10.1109/ITEC-AP.2014.6940781 (cit. on p. 13).